Piezoelectric Nanogenerators Based On BaTiO3 /PDMS Composites for High-Frequency Applications

Darya Meisak, Martynas Kinka, Artyom Plyushch, Jan Macutkevič, Aleksej Zarkov, Sébastien Schaefer, Algirdas Selskis, Vytautas Samulionis, Polina Kuzhir, Juras Banys, et al.

ACS OMEGA

http://pubs.acs.org/journal/acsodf

Article

Piezoelectric Nanogenerators Based On $BaTiO_3$/PDMS Composites for High-Frequency Applications

Darya Meisak,* Martynas Kinka, Artyom Plyushch, Jan Macutkevič, Aleksej Zarkov, Sébastien Schaefer, Algirdas Selskis, Vytautas Samulionis, Polina Kuzhir, Jūras Banys, Vanessa Fierro, and Alain Celzard

Cite This: *ACS Omega* 2023, 8, 13911−13919

Read Online

ACCESS | Metrics & More | Article Recommendations

ABSTRACT: A series of highly flexible and environmentally friendly composites based on polydimethylsiloxane (PDMS) filled with 200 nm size ferroelectric $BaTiO_3$ (BTO) particles at different concentrations (from 7 to 23 vol %) have been fabricated by a simple dispersion method. The dielectric, piezoelectric, and ultrasonic properties have been studied. The ferroelectric state of BTO was confirmed by differential scanning calorimetry and ultrasonic spectroscopy. The addition of BTO into PDMS strongly affects the dielectric properties of the composites. At low temperatures close to 160 K, the PDMS matrix exhibits a dielectric anomaly related to a dynamic glass transition, which shifts to higher temperatures as the BTO content increases due to the strong interaction between polymer chains and nanoparticles. Ultrasonic measurements demonstrate the appearance of a piezoelectric voltage signal on a thin plate of the composite with the highest available filler concentration (23 vol %) under longitudinal stress applied by a 10 MHz ultrasonic wave. As a result, at room temperature, the detected signal is characterized by output voltage and specific stored energy values of 10 mV and 367.3 MeV/m^2, respectively, followed by a further increase with cooling to 35 mV at 150 K. The proposed BTO/PDMS composite system is thus a potential candidate for nanogenerators, namely, a simple, flexible, and lead-free device converting high-frequency (10 MHz) mechanical vibrations into electrical voltage.

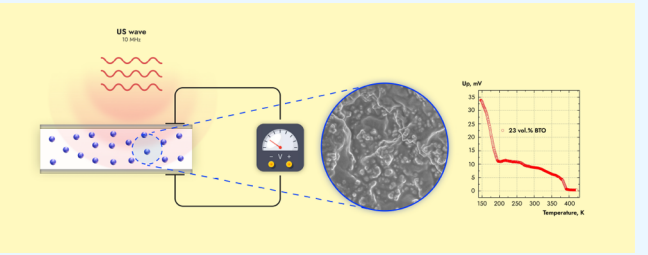

INTRODUCTION

The rapid decline of fossil fuels, as well as the resulting environmental pollution, has led to an active search for alternative "green" energy sources. Since piezoelectric (in 2007)[1] and triboelectric (in 2012)[2] nanogenerators were first mentioned, they have continued to receive attention due to the attractive prospect of creating efficient energy-harvesting devices by converting a ubiquitous energy source such as mechanical movement (acoustic waves, fluid flow, body deflection, compression, vibration, etc.) into useful electricity.[3−5]

Polymers, whether synthetic or organic, that are sufficiently elastic to respond to any mechanical pressure are ideal mediums for holding piezoelectric particles. Particularly, flexible polydimethylsiloxane (PDMS), which is chemically stable and exhibits a low glass transition temperature, simple processing, and durability in the cured state, has already been identified as one of the most popular polymers for nanogenerator design.[6−10] In turn, piezoelectric lead-free perovskite-type barium titanate $BaTiO_3$ is a balanced option in terms of environmental safety and a high piezoelectric coefficient.[6,9,11]

Thus, for more than a decade already there has been an active fight for every volt of output power, preferably with the simultaneous presence of other benefits, such as lightness, ease of large-scale fabrication, and low cost of the final product. The output performance of a nanogenerator based on polymer composite is determined, and therefore can be controlled, by many factors:[12] qualitative and quantitative compositions, homogeneity of filler distribution,[13,14] chemical doping,[15−19] morphology of the particles,[13,14,20,21] and 3D spatial ordering of particles in the matrix.[22−25] Regarding morphology, Jian et al.[14] obtained an output power value of 260 V for a PDMS-based system with hierarchical BTO flowers due to the high local stress at the petals, while for BTO in the form of nanoparticles,[20] nanowires,[21] and nanocubes[13] the values were 3.2, 7, and 126.3 V, respectively. Chemical doping was found to be an effective tool to adjust the piezoelectric coefficients of the materials and increase their ability to harvest energy.[15−19] Besides, the load transfer efficiency can also be improved by forming three-dimensional (3D) skeletons, such as foams,[22]

Received: January 16, 2023
Accepted: March 27, 2023
Published: April 6, 2023

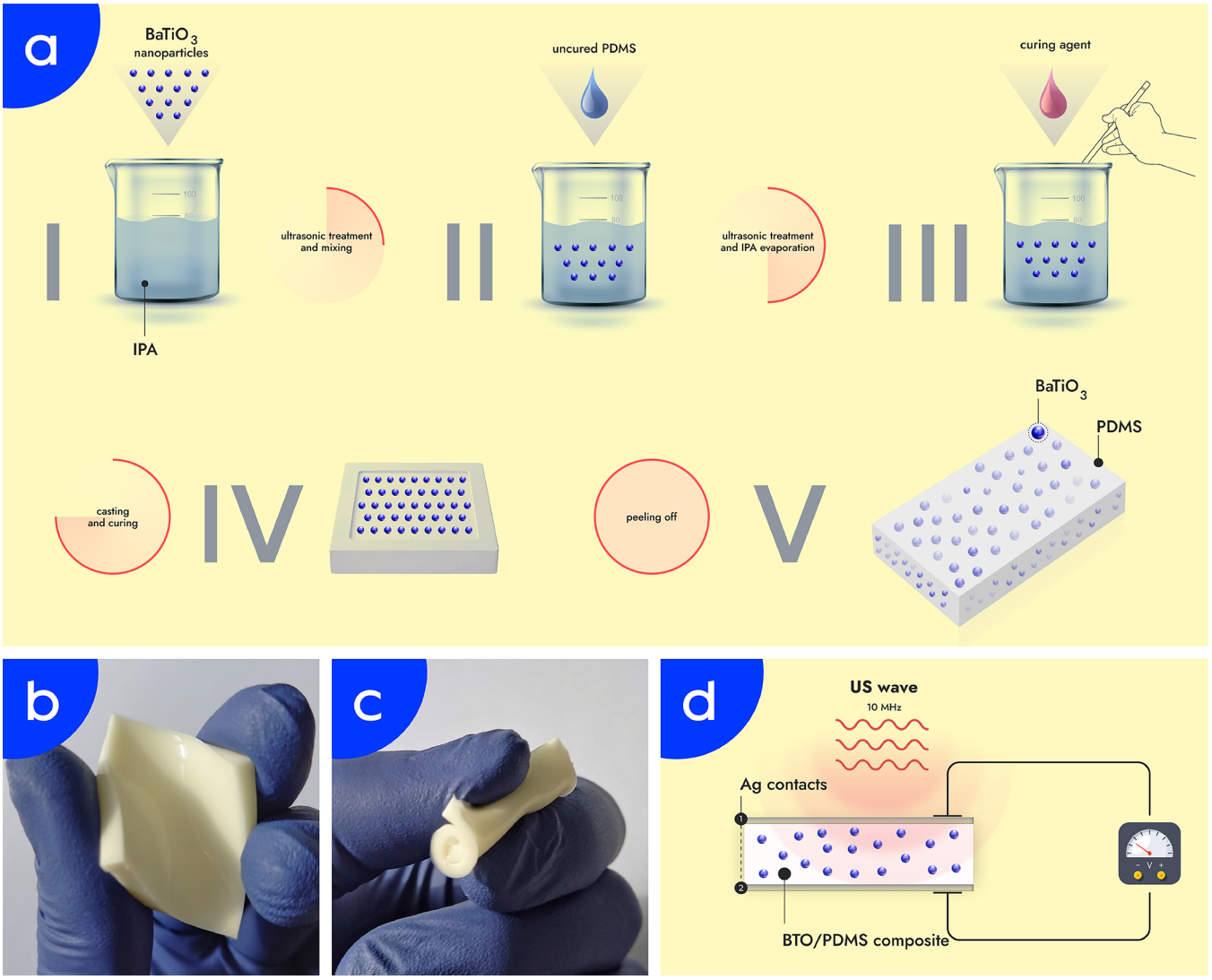

Figure 1. (a) Preparation procedure for BTO/PDMS composites. (b and c) Images demonstrating the flexibility and winding capabilities of the BTO/PDMS composites. (d) Schematic representation of an experiment to measure the piezoelectric voltage.

porous aerogels,[23,24] and sponge-like structures.[25] Finally, hybrid nanogenerators, which operate using both tribo- and piezoelectric effects, demonstrate enhanced output characteristics.[26−28]

However, most research is devoted to the quasi-static frequency range (i.e., less than 100 Hz). The latter corresponds to wasted tiny biomechanical motions and wind and water vibrations, while for many existing devices nanogenerators could be beneficial for converting high-frequency vibrations (e.g., from cars, aircrafts, and electric engines) into useful electrical energy. Besides, the majority of studies on mechanical energy harvesting mainly cover the region of room temperature without data on a parameter as important for defining the properties of any material as the dielectric permittivity, and its complex investigation as a function of temperature and frequency is extremely rare.[28] Therefore, to fill the gaps, the current study aims to perform complex investigations (dielectric and ultrasonic) on composite systems containing ferroelectric barium titanate ($BaTiO_3$) nanoparticles in a polydimethylsiloxane (PDMS) polymer matrix in order to determine their suitability as nanogenerators for high-frequency (10 MHz) applications.

MATERIALS AND METHODS

Materials. Commercially available barium titanate ($BaTiO_3$ or BTO) nanoparticles of 200 nm size from Sigma-Aldrich were used. Polydimethylsiloxane (PDMS), namely, Sylgard 184 silicone elastomer, was purchased from Dow-Corning (Midland, MI, USA) as a two-part material consisting of a base and a curing agent.

Composite Preparation. The composites were prepared as follows (see Figure 1a): BTO particles were dispersed in isopropyl alcohol (IPA) using sonication for 3 h to break up the agglomerates. Next, the PDMS base was introduced into the solution, and the resulting mixture was sonicated for another 3 h. After a homogeneous dispersion was obtained, the system was placed in an oven for alcohol removal. After the addition of the curing agent, the blend was gently stirred manually for 5 min and poured into the mold for the curing process. Finally, the composites were cured at 333 K for 2 h and at 313 K overnight. Following this protocol, samples with 7, 11, 15, and 23 vol % BTO dispersed in the PDMS matrix were prepared. The obtained composites exhibit remarkable flexibility and winding properties (see Figure 1b and c),

https://doi.org/10.1021/acsomega.3c00321
ACS Omega 2023, 8, 13911−13919

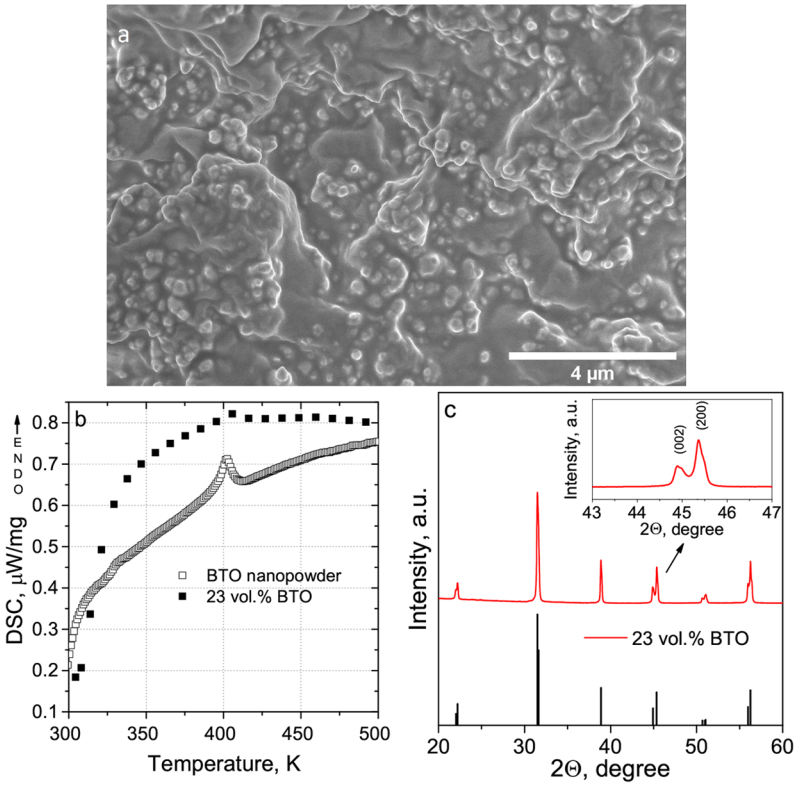

Figure 2. (a) Scanning electron microscopy (SEM) image of the 23 vol % BTO/PDMS composite. (b) Differential scanning calorimetry curves of BTO nanopowder and the 23 vol % BTO/PDMS composite. (c) X-ray diffraction pattern of the 23 vol % BTO/PDMS composite at room temperature.

making them suitable for flexible energy-harvesting applications.

Characterization and Measurements. The complex dielectric permittivity of the samples was measured in the frequency range from 20 Hz to 1 MHz using an HP4284A LCR meter. In the frequency range of 10−300 MHz, dielectric measurements were performed by a coaxial dielectric spectrometer with an Agilent 8714ET vector network analyzer. For measurements above room temperature, a lab-made furnace was used, while for lower temperatures a liquid nitrogen cooling system was applied. Samples with a typical thickness of 1.5 mm and a cross-sectional area of 2 mm^2 with pre-applied silver paste as electrical contacts were studied.

Ultrasonic wave attenuation and velocity data were obtained using a standard pulse-echo ultrasonic measurement setup with a computer-controlled RITEC RAM-5000 pulse-echo ultrasonic measurement system.[29,30] Z-Cut lithium niobate $LiNbO_3$ piezoelectric transducers were used for excitation and the detection of longitudinal ultrasonic waves at 10 MHz. The typical sample thickness was 2−3 mm, and the heating/cooling rate was kept below 1 K/min. Silicon oil was applied between the sample, quartz buffer rods, and transducers to maintain acoustic bonds throughout the entire measured temperature range.

In the case of piezoelectric measurements, a longitudinal ultrasonic wave was detected by a thinly cut 0.2 mm thick sample functioning as a receiving transducer. First, the sample was heated above 400 K and slowly cooled to 150 K in a DC bias field of 20 kV/cm (so that the total polarization time was 4 h). Then, the poling field was removed and the piezoelectric voltage in the form of a 10 MHz radio-pulse signal detected by the sample was measured by an Agilent DSO3202A digital scope incorporated in the electronic pulse-echo setup for automatic temperature measurements. A very simple schematic representation of an experiment for piezoelectric voltage measurement is presented in Figure 1(d).

The measurement of heat fluxes through the barium titanate nanopowder on the one hand, and its PDMS matrix composite on the other hand, when heated at a constant rate of 10 K/min was performed with the DSC (differential scanning calorimetry) accessory of a NETZSCH STA 449 F3 Jupiter thermogravimetric apparatus. To do this, samples of a few milligrams, carefully weighed beforehand, were installed in an aluminum crucible, the reference crucible being empty, and the whole was heated between room temperature and 500 K under a nitrogen flow. The signal from the thermocouples was directly recorded in units of μW/mg but was not calibrated to deduce the corresponding changes in heat capacity, absolute values of which were not considered necessary in this context.

The structural and morphological properties of the samples were studied by scanning electron microscopy (SEM) using a Helios NanoLab 650 microscope (Thermo Fisher Scientific, Hillsboro, OR) with a TLD-SE detector and an acceleration voltage of 3 kV.

X-ray diffraction (XRD) analysis was carried out on a Rigaku MiniFlex II diffractometer using Cu Kα radiation (λ = 1.5419 Å) working in the Bragg−Brentano ($\theta/2\theta$) geometry. The data were collected over a 2θ angle range of 10−60° with a speed of 1°/min.

https://doi.org/10.1021/acsomega.3c00321
ACS Omega 2023, 8, 13911−13919

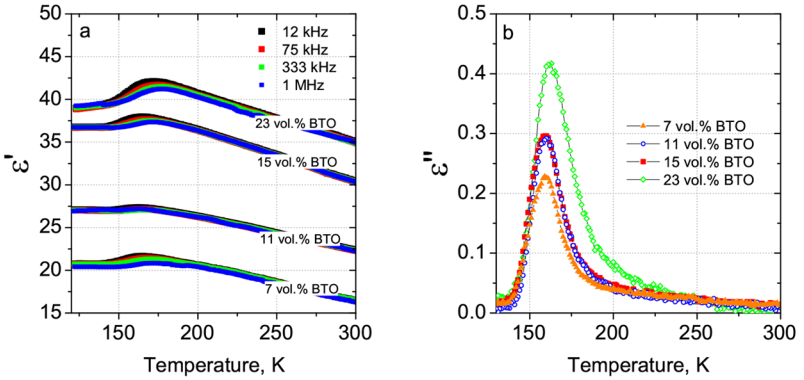

Figure 3. Temperature dependencies (below RT) of (a) the real part of the dielectric permittivity at different frequencies, and (b) the imaginary part at the 75 kHz frequency for 7, 11, 15, and 23 vol % BTO/PDMS composites.

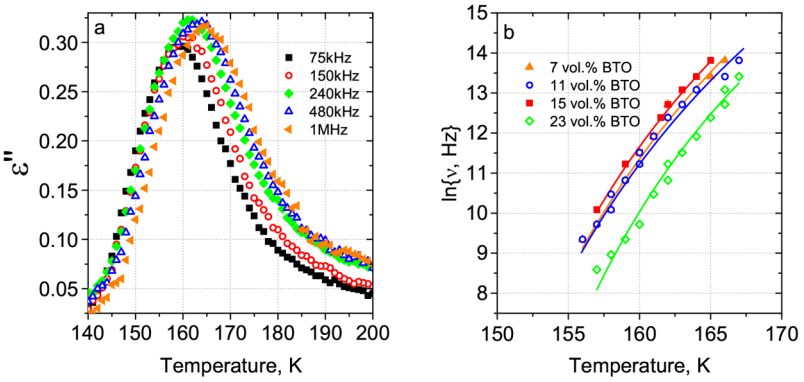

Figure 4. (a) Typical temperature dependencies of dielectric losses at different frequencies, illustrated by that of the BTO/PDMS composite at 15 vol % taken as an example. (b) Frequency at maximum dielectric losses measured as a function of temperature for BTO/PDMS composites at 7, 11, 15, and 23 vol % . The solid lines are the best fits according to the Vogel–Fulcher equation (eq 1).

RESULTS AND DISCUSSION

Characterizations of BTO/PDMS Composites. The volume distribution of BTO nanoparticles within the PDMS matrix is quite homogeneous, as can be seen in the scanning electron microscopy (SEM) image (Figure 2a) for the composite with the maximum available filler concentration of 23 vol %. Differential scanning calorimetry (DSC) analysis was performed for the BTO nanopowder and the 23 vol % BTO/PDMS composite (see Figure 2b). The peak near 400 K for both curves is associated with a ferroelectric–paraelectric second-order phase transition, which reveals the ferroelectric ordering of $BaTiO_3$. The latter is also confirmed by the XRD pattern obtained at room temperature for the 23 vol % BTO/PDMS composite (see Figure 2c). All peaks are identified as the *P4mm* $BaTiO_3$ tetragonal (PDF-2 no. 00-081-2201) phase (Figure 2c, black symbols). The peak near 45° is characterized by a splitting, which corresponds to the reflections from the (002) and (200) planes of $BaTiO_3$ (see the inset in Figure 2c). This indicates the tetragonal distortion of the $BaTiO_3$ crystal lattice typical of the ferroelectric state.[31,32] Although the considered $BaTiO_3$ grain size of 200 nm is close to the critical size, which means that presumably at least some of the smaller grains are cubic at room temperature, the observed splitting proves the presence of the ferroelectric phase as well.

Dielectric Properties below Room Temperature. The temperature dependencies (below room temperature) of the real part of the complex dielectric permittivity at different frequencies for all studied BTO/PDMS composites are presented in Figure 3a, while the imaginary parts as a function of temperature at 75 kHz are presented in Figure 3b.

The permittivity at room temperature (300 K) is characterized by two features: on the one hand, an increase in the value of the real part with the loading of BTO particles, and on the other hand a frequency independence. However, at low temperatures close to 160 K, an anomalous behavior is detected, which is associated with α-relaxation, also called the dynamic glass transition of PDMS.[33,34] Considering the thermal behavior of pure PDMS,[35] the increase in BTO content is manifested by a shift of the dielectric loss to higher temperatures. Besides, the position of the peak considered for each particular sample is frequency-dependent (see Figure 4a for a 15 vol % BTO/PDMS composite). Namely, as frequency ν increases, the maximum shifts to higher temperatures according to the Vogel–Fulcher law (see Figure 4b):[36]

$$\nu = \nu_0 \exp \frac{-E_{VF}}{k_B(T_{max} - T_{ref})} \quad (1)$$

where T_{ref} is the glass transition temperature of the polymer, T_{max} is the temperature at which the dielectric losses are the highest, k_B is the Boltzmann constant, ν_0 is the frequency at very high T_{max}, and E_{VF} is the activation energy.

The parameters of the best fits to the experimental data for all BTO/PDMS composites are presented in Table 1 (marked by superscript (1)). In the composites, according to Table 1, the glass transition temperature increases with the concentration of BTO particles, while the activation energy decreases.

https://doi.org/10.1021/acsomega.3c00321
ACS Omega 2023, 8, 13911–13919

Table 1. Glass Transition Temperatures and Vogel–Fulcher Activation Energies of BTO/PDMS Composites

BTO, vol %	ν_0, THz	$E_{VF}^{(1)}/k_B$, K	$T_{ref}^{(1)}$, K	τ_0, ns	$E_{VF}^{(2)}/k_B$, K	$T_{ref}^{(2)}$, K
7	4.8	642.7	123.9	0.06	433.9	121.8
11	1.18	575.6	125.3	0.1	399.3	124.8
15	0.88	512.4	127.7	0.17	347.0	125.5
23	0.18	437.7	132.5	0.27	328.7	130.0

This increase in T_{ref} is related to the slowing of local segmental dynamics,[37] i.e., to the reduction of the mobility of polymer chains located near the filler due to strong interfacial interactions. Similar behavior has been frequently observed in various PDMS-based composite systems.[35,38−40]

The frequency spectra at a temperature close to the glass transition also exhibit relaxation behavior, namely, a maximum of the imaginary part of the dielectric permittivity is observed. Figure 5a shows the frequency dependencies of ε'' for a 15 vol % BTO/PDMS composite at different temperatures.

To analyze the frequency spectra of ε'', the Cole–Cole equation[41] can be used (see solid lines on Figure 5a):

$$\varepsilon^*(\omega) = \varepsilon_\infty + \frac{\Delta\varepsilon}{1 + (i\omega\tau)^{1-\alpha}} \quad (2)$$

where $\varepsilon^* = \varepsilon' - i\varepsilon''$ is the complex dielectric permittivity, ε_∞ is the dielectric permittivity at infinite frequency, $\Delta\varepsilon$ is the dielectric strength (i.e., the difference between the static dielectric permittivity and ε_∞), τ is the relaxation time, ω is the angular frequency defined as $\omega = 2\pi\nu$, and α is the parameter responsible for the width of the relaxation time distribution.

The fitted parameters α and ε_∞ were found to be weakly dependent on temperature in the considered range from 150 to 170 K, while the relaxation time increased with cooling. The obtained τ values can be plotted as a function of temperature and then fitted according to the Vogel–Fulcher equation (eq 1), taking into account the reciprocal relationship between τ and the relaxation frequency ν_r, i.e., $\tau = 1/\nu_r$. The temperature dependencies of the relaxation time, as well as the best Vogel–Fulcher fits for all the composites investigated, are presented in Figure 5b. The relaxation time fitting parameters are collected in Table 1 (marked by superscript (2)) and are in agreement with the data obtained using the $\varepsilon''(T)$ dependencies because the dielectric dispersion is very narrow.

As a result, due to the strong interactions between BTO nanoparticles and PDMS polymer chains, the properties of the composites can be adjusted by controlling the BTO concentration. In particular, the glass transition temperature monotonously shifts to higher temperatures as the BTO content increases.

Dielectric Properties above Room Temperature. Dielectric measurements for higher temperatures (above room temperature) have also been performed, and the corresponding temperature dependencies of the real part of the complex dielectric permittivity at the frequency of 1 MHz for all composites studied are presented in Figure 6a. In this case, there is no need to show the $\varepsilon'(T)$ dependencies at different frequencies as in Figure 3a, since the frequency dispersion of the dielectric spectra is absent far from the glass transition. This fact is also confirmed by the broadband spectra shown in Figure 6b for the 23 vol % BTO/PDMS composite at different temperatures in a wide range including low (20 Hz to 1 MHz) and high (10–300 MHz) frequencies. Thus, for all concentrations considered, ε' is characterized by a monotonic decrease with heating.

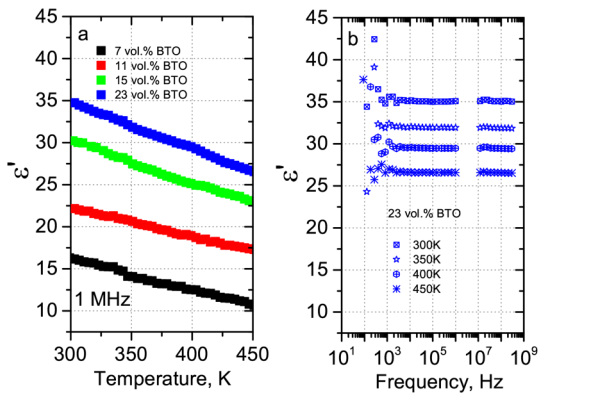

Figure 6. (a) Temperature dependence (above RT) of the real part of the dielectric permittivity at the frequency of 1 MHz for the 7, 11, 15, and 23 vol % BTO/PDMS composites. (b) Frequency dependence (from 20 Hz to 300 MHz) of the real part of the dielectric permittivity for the 23 vol % BTO/PDMS composite at different temperatures.

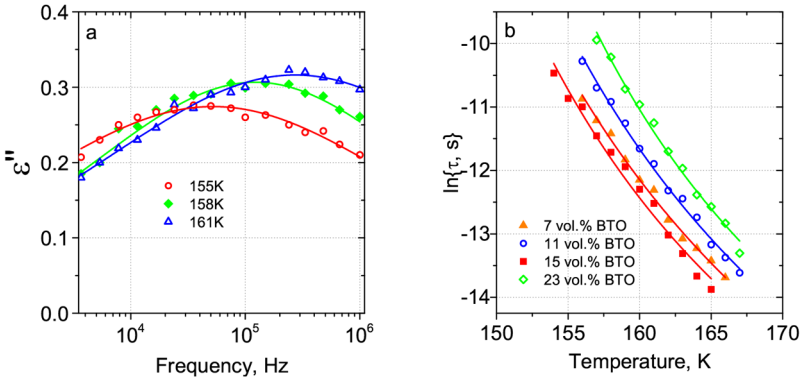

Figure 5. (a) Frequency spectra of the imaginary part of the dielectric permittivity at different temperatures for the 15 vol % BTO/PDMS composite. The solid lines are the best fits according to the Cole–Cole equation (eq 2). (b) Temperature dependencies of the relaxation time obtained from Cole–Cole fits for the 7, 11, 15, and 23 vol % BTO/PDMS composites. The solid lines are the best fits according to the Vogel–Fulcher equation (eq 1).

https://doi.org/10.1021/acsomega.3c00321
ACS Omega 2023, 8, 13911−13919

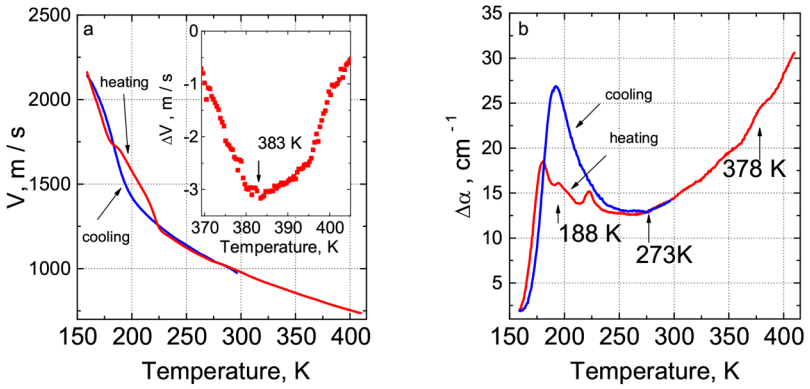

Figure 7. Temperature dependencies of (a) the ultrasonic wave velocity and (b) the ultrasonic wave attenuation measured at a frequency of 10 MHz for the 23 vol % BTO/PDMS composite upon cooling (blue curve) and heating (red curve).

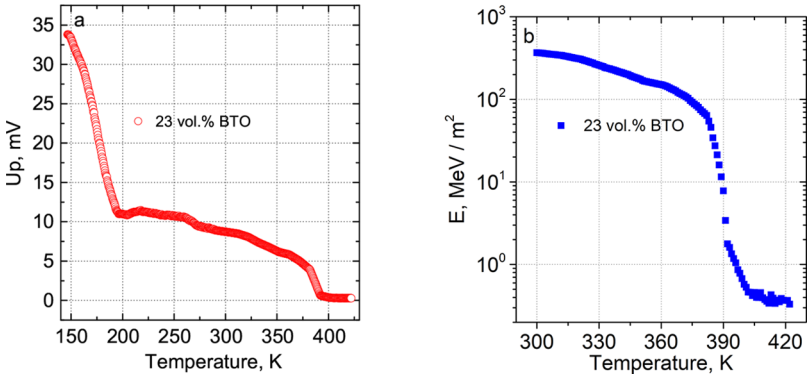

Figure 8. Temperature dependencies of (a) the piezoelectric voltage signal and (b) the specific stored energy at a frequency of 10 MHz for a 23 vol % BTO/PDMS composite of 0.2 mm thickness.

Piezoelectric Properties. To investigate the influence of BTO nanoparticles on the glass transition and freezing–melting dynamics of the PDMS-based composite, ultrasonic measurements have been performed. The longitudinal ultrasonic wave velocity V and attenuation values $\Delta\alpha$ were measured at a frequency of 10 MHz upon cooling from room temperature to 150 K and upon subsequent heating to 430 K. The results for the highest available concentration of 23% of BTO in the PDMS-based composite are presented in Figure 7a and b.

Upon cooling, the anomalous temperature behavior of both V and $\Delta\alpha$ is centered around 190 K. This anomaly has a characteristic shape usually observed in the crossing of the glass transition, where the steepest velocity dispersion region corresponds to the attenuation maximum.[42] In glass formation and other systems with strong dynamic relaxation, the sound velocity and attenuation are also frequency-dependent. Such systems, when probed ultrasonically, are less rigid on time scales greater than the stress relaxation time (in contrast to much shorter time scales), and the energy dissipation is the highest when the probing frequency is close to the inverse value of the relaxation time. Upon heating, the $\Delta\alpha$ maximum splits into two peaks, indicating a sequence of glassy and semicrystalline/amorphous transitions, which have also been observed in other PDMS-based systems, particularly with ZnO[39] and OLC (onion-like carbon)[43] nanoinclusions. The smaller PDMS crystallites begin to melt, while the larger ones remain large enough to preserve the stiff structure of the glassy elastomer.[44] When this structure finally collapses, the longitudinal velocity (Figure 7a) begins to decrease further again, resulting in a step-like temperature dependence.

Between the two mentioned attenuation peaks of the glass transition and semicrystalline melting in the PDMS matrix, a third one at 188 K has been observed. This temperature value is close to the rhombohedral–orthorhombic phase transition in the BTO bulk material. However, this anomaly cannot be attributed to the BTO phase transition based solely on V and $\Delta\alpha$ measurements, as no corresponding velocity anomalies were observed in this or higher regions. It is only at high temperatures around 380 K that a small and broad $\Delta\alpha$ maximum, with an associated anomalous ultrasonic velocity slow down (see Figure 7a(inset)), suggests a possible ferroelectric to paraelectric phase transition in BTO nanoparticles. To obtain a more stringent evidence for the formation of a ferroelectric state, as well as to evaluate the suitability of the 23 vol % BTO/PDMS composite as a high-frequency piezo-nanogenerator, some additional ultrasonic measurements of the piezoelectric properties at 10 MHz have been performed.

The temperature dependence of the piezoelectric voltage signal U_p arising on a piezoelectric plate under longitudinal stress applied by the ultrasonic wave is presented in Figure 8a. The U_p signal decreases upon heating, and distinct anomalies appear at the temperatures of the phase transitions in the BTO bulk: the signal drops to a value of 10 V at 190 K, followed by a small kink around 273 K, and disappears completely in the paraelectric phase above 390 K. Samples at lower concen-

https://doi.org/10.1021/acsomega.3c00321
ACS Omega 2023, 8, 13911−13919

tration showed no piezoelectric signal (so no data are presented). This means that the BTO grains do not percolate.

By having data on the voltage across the capacitor plates (U), as well as the dielectric permittivity of the capacitor space-filling material (ε), the stored energy E of such a system can be estimated. For this purpose, the following simple formula $E = \frac{CU^2}{2}$ can be applied. Here, the capacitance C in the case of a flat capacitor is defined as $C = \varepsilon\varepsilon_0 S/d$, where ε_0 is the permittivity of vacuum, S is the area of the capacitor plates, and d is the distance between them. The temperature dependence of the specific energy stored by a flat capacitor with a potential difference U_p filled with a 0.2 mm-thick 23 vol % BTO/PDMS composite is presented in Figure 8b. Due to the noisy results of the temperature measurements in the 10−300 MHz frequency range, for the energy calculations, the data at 1 MHz (blue curve in Figure 6a) were legitimately taken, since the frequency dispersion is absent far from the glass transition (see Figure 6b).

Thus, a 0.2 mm-thick piezoelectric plate of the 23 vol % BTO/PDMS composite converts high-frequency mechanical vibrations in the form of a 10 MHz ultrasonic wave into an electrical signal with an output voltage of 10 mV and a specific stored energy of 367.3 MeV/m^2 at room temperature, which reaches 35 mV after the glass transition of PDMS. The measured value of the output voltage is lower[13,14,20,21] due to two factors: (i) the increase in frequency from quasi-static to MHz, which reduces the piezoelectric coefficient, and (ii) the low power of ultrasonic excitation.

CONCLUSIONS

In summary, using a simple dispersion method, a series of flexible composites with ferroelectric BTO nanoparticles at different concentrations (7−23 vol %) in a PDMS matrix have been prepared. The dielectric, piezoelectric, and ultrasonic properties of the obtained composites have been studied. At high temperatures, the dielectric permittivity spectra of the BTO/PDMS composites are frequency-independent over a wide range, while at low temperatures a pronounced anomaly appears that is associated with the dynamic glass transition in PDMS. Moreover, due to the strong interaction between PDMS chains and BTO nanoparticles, the glass transition temperature derived from the Vogel−Fulcher law shifts to higher temperatures from 121.8 to 130 K with the increasing BTO content (from 7 to 23 vol %). Ultrasonic measurements at 10 MHz also confirm the presence of the glass transition of the polymer, which is expressed by the steepest wave velocity dispersion and attenuation maximum near the transition temperature. Additionally, the composites have been checked for piezoelectric response under longitudinal stress applied by a 10 MHz ultrasonic wave: below 400 K, the piezoelectric voltage signal appears only for a sample with the highest concentration (23 vol %), while for the others the signal is absent. The output voltages are 10 and 35 mV above the glass transition and in the glass state, respectively. Having the dielectric permittivity data of the material, the value of the specific stored energy has been estimated and, in the particular case of room temperature, it is 367.3 MeV/m^2. The output characteristics are not very high due to the low power of ultrasonic excitation and the decrease in the piezoelectric coefficient as the frequency increases. It is expected that the use of more powerful vibration sources will lead to a significant increase in the output voltage. The BTO/PDMS composite system is a prospective candidate for high-frequency nanogenerator and energy harvester applications.

AUTHOR INFORMATION

Corresponding Author

Darya Meisak − *Faculty of Chemistry and Geosciences, Vilnius University, Vilnius LT-03225, Lithuania; Faculty of Physics, Vilnius University, Vilnius LT-10222, Lithuania;* orcid.org/0000-0002-6249-2181; Email: darya.meisak@ff.vu.lt

Authors

Martynas Kinka − *Faculty of Physics, Vilnius University, Vilnius LT-10222, Lithuania*

Artyom Plyushch − *Faculty of Physics, Vilnius University, Vilnius LT-10222, Lithuania*

Jan Macutkevič − *Faculty of Physics, Vilnius University, Vilnius LT-10222, Lithuania*

Aleksej Zarkov − *Faculty of Chemistry and Geosciences, Vilnius University, Vilnius LT-03225, Lithuania;* orcid.org/0000-0002-3574-2296

Sébastien Schaefer − *CNRS, IJL, Université de Lorraine, Epinal F-88000, France;* orcid.org/0000-0002-6299-0340

Algirdas Selskis − *Center for Physical Science and Technology, Vilnius LT-10257, Lithuania*

Vytautas Samulionis − *Faculty of Physics, Vilnius University, Vilnius LT-10222, Lithuania*

Polina Kuzhir − *Institute of Photonics, University of Eastern Finland, Joensuu FI-80101, Finland*

Jūras Banys − *Faculty of Physics, Vilnius University, Vilnius LT-10222, Lithuania*

Vanessa Fierro − *CNRS, IJL, Université de Lorraine, Epinal F-88000, France;* orcid.org/0000-0001-7081-3697

Alain Celzard − *CNRS, IJL, Université de Lorraine, Epinal F-88000, France; Institut Universitaire de France (IUF), 75231 Paris, France;* orcid.org/0000-0003-0073-9545

Complete contact information is available at: https://pubs.acs.org/10.1021/acsomega.3c00321

Notes

The authors declare no competing financial interest.

ACKNOWLEDGMENTS

D.M. has received funding from the Research Council of Lithuania (LMTLT), agreement no S-PD-22-90. J.M., S.S., V.F., and A.C. acknowledge funding from the NATO Science for Peace and Security Program (Grant G5697 CERTAIN "Globular carbon-based structures and metamaterials for enhanced electromagnetic protection"). P.K. is supported by the Academy of Finland via the Flagship Programme Photonics Research and Innovation (PREIN), decision 320166, and by the Horizon 2020 RISE DiSeTCom Project 823728. The authors thank Victoria Kravchenko and Aliaksei Sokal for valuable discussions.

REFERENCES

(1) Wang, X.; Song, J.; Liu, J.; Wang, Z. L. Direct-current nanogenerator driven by ultrasonic waves. *Science* **2007**, *316*, 102−105.

(2) Fan, F.-R.; Tian, Z.-Q.; Wang, Z. L. Flexible triboelectric generator. *Nano Energy* **2012**, *1*, 328−334.

(3) Torres, F. G.; De-la Torre, G. E. Polysaccharide-based triboelectric nanogenerators: a review. *Carbohydr. Polym.* **2021**, *251*, 117055.
(4) Briscoe, J.; Dunn, S. Piezoelectric nanogenerators—a review of nanostructured piezoelectric energy harvesters. *Nano Energy* **2015**, *14*, 15−29.
(5) Mahapatra, B.; Kumar Patel, K.; Vidya; Patel, P. K.; et al. A review on recent advancement in materials for piezoelectric/triboelectric nanogenerators. *Mater. Today: Proc.* **2021**, *46*, 5523−5529.
(6) Nayak, S.; Chaki, T. K.; Khastgir, D. Development of flexible piezoelectric poly (dimethylsiloxane)-BaTiO3 nanocomposites for electrical energy harvesting. *Ind. Eng. Chem. Res.* **2014**, *53*, 14982−14992.
(7) Li, G.-Z.; Wang, G.-G.; Ye, D.-M.; Zhang, X.-W.; Lin, Z.-Q.; Zhou, H.-L.; Li, F.; Wang, B.-L.; Han, J.-C. High-performance transparent and flexible triboelectric nanogenerators based on PDMS-PTFE composite films. *Adv. Electron. Mater.* **2019**, *5*, 1800846.
(8) Ren, X.; Fan, H.; Zhao, Y.; Liu, Z. Flexible lead-free BiFeO3/PDMS-based nanogenerator as piezoelectric energy harvester. *ACS Appl. Mater. Interfaces* **2016**, *8*, 26190−26197.
(9) Zhang, G.; Liao, Q.; Zhang, Z.; Liang, Q.; Zhao, Y.; Zheng, X.; Zhang, Y. Novel piezoelectric paper-based flexible nanogenerators composed of batio3 nanoparticles and bacterial cellulose. *Adv. Sci.* **2016**, *3*, 1500257.
(10) Sun, Q.-J.; Lei, Y.; Zhao, X.-H.; Han, J.; Cao, R.; Zhang, J.; Wu, W.; Heidari, H.; Li, W.-J.; Sun, Q.; et al. Scalable fabrication of hierarchically structured graphite/polydimethylsiloxane composite films for large-area triboelectric nanogenerators and self-powered tactile sensing. *Nano Energy* **2021**, *80*, 105521.
(11) Lin, Z.-H.; Yang, Y.; Wu, J. M.; Liu, Y.; Zhang, F.; Wang, Z. L. BaTiO3 nanotubes-based flexible and transparent nanogenerators. *J. Phys. Chem. Lett.* **2012**, *3*, 3599−3604.
(12) Hu, D.; Yao, M.; Fan, Y.; Ma, C.; Fan, M.; Liu, M. Strategies to achieve high performance piezoelectric nanogenerators. *Nano Energy* **2019**, *55*, 288−304.
(13) Alluri, N. R.; Chandrasekhar, A.; Vivekananthan, V.; Purusothaman, Y.; Selvarajan, S.; Jeong, J. H.; Kim, S.-J. Scavenging biomechanical energy using high-performance, flexible BaTiO3 nanocube/PDMS composite films. *ACS Sustainable Chem. Eng.* **2017**, *5*, 4730−4738.
(14) Jian, G.; Jiao, Y.; Meng, Q.; Shao, H.; Wang, F.; Wei, Z. 3D BaTiO3 flower based polymer composites exhibiting excellent piezoelectric energy harvesting properties. *Adv. Mater. Interfaces* **2020**, *7*, 2000484.
(15) Alluri, N. R.; Saravanakumar, B.; Kim, S.-J. Flexible, hybrid piezoelectric film (BaTi (1-x) Zr x O3)/PVDF nanogenerator as a self-powered fluid velocity sensor. *ACS Appl. Mater. Interfaces* **2015**, *7*, 9831−9840.
(16) Baek, C.; Wang, J. E.; Ryu, S.; Kim, J.-H.; Jeong, C. K.; Park, K.-I.; Kim, D. K. Facile hydrothermal synthesis of BaZr x Ti 1- x O 3 nanoparticles and their application to a lead-free nanocomposite generator. *RSC Adv.* **2017**, *7*, 2851−2856.
(17) Yan, J.; Jeong, Y. G. Roles of carbon nanotube and BaTiO3 nanofiber in the electrical, dielectric and piezoelectric properties of flexible nanocomposite generators. *Compos. Sci. Technol.* **2017**, *144*, 1−10.
(18) Luo, C.; Hu, S.; Xia, M.; Li, P.; Hu, J.; Li, G.; Jiang, H.; Zhang, W. A Flexible Lead-Free BaTiO3/PDMS/C Composite Nanogenerator as a Piezoelectric Energy Harvester. *Energy Technol.* **2018**, *6*, 922−927.
(19) Wu, Y.; Ma, F.; Qu, J.; Luo, Y.; Lv, C.; Guo, Q.; Qi, T. Vertically-aligned lead-free BCTZY nanofibers with enhanced electrical properties for flexible piezoelectric nanogenerators. *Appl. Surf. Sci.* **2019**, *469*, 283−291.
(20) Park, K.-I.; Lee, M.; Liu, Y.; Moon, S.; Hwang, G.-T.; Zhu, G.; Kim, J. E.; Kim, S. O.; Kim, D. K.; Wang, Z. L.; et al. Flexible nanocomposite generator made of BaTiO3 nanoparticles and graphitic carbons. *Adv. Mater.* **2012**, *24*, 2999−3004.
(21) Tsege, E. L.; Kim, G. H.; Annapureddy, V.; Kim, B.; Kim, H.-K.; Hwang, Y.-H. A flexible lead-free piezoelectric nanogenerator based on vertically aligned BaTiO 3 nanotube arrays on a Ti-mesh substrate. *RSC Adv.* **2016**, *6*, 81426−81435.
(22) Zhang, G.; Zhao, P.; Zhang, X.; Han, K.; Zhao, T.; Zhang, Y.; Jeong, C. K.; Jiang, S.; Zhang, S.; Wang, Q. Flexible three-dimensional interconnected piezoelectric ceramic foam based composites for highly efficient concurrent mechanical and thermal energy harvesting. *Energy Environ. Sci.* **2018**, *11*, 2046−2056.
(23) Su, H.; Wang, X.; Li, C.; Wang, Z.; Wu, Y.; Zhang, J.; Zhang, Y.; Zhao, C.; Wu, J.; Zheng, H. Enhanced energy harvesting ability of polydimethylsiloxane-BaTiO3-based flexible piezoelectric nanogenerator for tactile imitation application. *Nano Energy* **2021**, *83*, 105809.
(24) Zheng, Q.; Zhang, H.; Mi, H.; Cai, Z.; Ma, Z.; Gong, S. High-performance flexible piezoelectric nanogenerators consisting of porous cellulose nanofibril (CNF)/poly (dimethylsiloxane)(PDMS) aerogel films. *Nano Energy* **2016**, *26*, 504−512.
(25) Mao, Y.; Zhao, P.; McConohy, G.; Yang, H.; Tong, Y.; Wang, X. Sponge-like piezoelectric polymer films for scalable and integratable nanogenerators and self-powered electronic systems. *Adv. Energy Mater.* **2014**, *4*, 1301624.
(26) Sriphan, S.; Charoonsuk, T.; Maluangnont, T.; Vittayakorn, N. High-performance hybridized composited-based piezoelectric and triboelectric nanogenerators based on BaTiO3/PDMS composite film modified with Ti0. 8O2 nanosheets and silver nanopowders cofillers. *ACS Appl. Energy Mater.* **2019**, *2*, 3840−3850.
(27) Suo, G.; Yu, Y.; Zhang, Z.; Wang, S.; Zhao, P.; Li, J.; Wang, X. Piezoelectric and triboelectric dual effects in mechanical-energy harvesting using BaTiO3/polydimethylsiloxane composite film. *ACS Appl. Mater. Interfaces* **2016**, *8*, 34335−34341.
(28) Hajra, S.; Padhan, A. M.; Sahu, M.; Alagarsamy, P.; Lee, K.; Kim, H. J. Lead-free flexible Bismuth Titanate-PDMS composites: A multifunctional colossal dielectric material for hybrid piezo-triboelectric nanogenerator to sustainably power portable electronics. *Nano Energy* **2021**, *89*, 106316.
(29) Samulionis, V.; Banys, J.; Vysochanskii, Y. Piezoelectric and elastic properties of layered materials of Cu (In, Cr) P2 (S, Se) 6 system. *J. Electroceram.* **2009**, *22*, 192−197.
(30) Samulionis, V.; Banys, J.; Vysochanskii, Y. Ultrasonic and piezoelectric studies of phase transitions in two-dimensional CuInP2S6 type crystals. *Ferroelectrics* **2009**, *379*, 69−76.
(31) Manika, G. C.; Andrikopoulos, K. S.; Psarras, G. C. On the ferroelectric to paraelectric structural transition of BaTiO3 micro-/nanoparticles and their epoxy nanocomposites. *Molecules* **2020**, *25*, 2686.
(32) Wang, Z.-m.; Zhao, K.; Guo, X.-l.; Sun, W.; Jiang, H.-l.; Han, X.-q.; Tao, X.-t.; Cheng, Z.-x.; Zhao, H.-y.; Kimura, H.; et al. Crystallization, phase evolution and ferroelectric properties of sol-gel-synthesized Ba (Ti 0.8 Zr 0.2) O 3−x (Ba 0.7 Ca 0.3) TiO 3 thin films. *J. Mater. Chem. C* **2013**, *1*, 522−530.
(33) Klonos, P. A. Crystallization, glass transition, and molecular dynamics in PDMS of low molecular weights: A calorimetric and dielectric study. *Polymer* **2018**, *159*, 169−180.
(34) Bosq, N.; Guigo, N.; Persello, J.; Sbirrazzuoli, N. Melt and glass crystallization of PDMS and PDMS silica nanocomposites. *Phys. Chem. Chem. Phys.* **2014**, *16*, 7830−7840.
(35) Plyushch, A.; Macutkevič, J.; Banys, J.; Kuzhir, P.; Kalanda, N.; Petrov, A.; Silvestre, C.; Uimin, M. A.; Yermakov, A. Y.; Shenderova, O. Carbon-coated nickel nanoparticles: Effect on the magnetic and electric properties of composite materials. *Coatings* **2018**, *8*, 165.
(36) Vogel, H. The law of the relation between the viscosity of liquids and the temperature. *Phys. Z.* **1921**, *22*, 645−646.
(37) Robertson, C. G.; Roland, C. Glass transition and interfacial segmental dynamics in polymer-particle composites. *Rubber Chem. Technol.* **2008**, *81*, 506−522.
(38) Fragiadakis, D.; Pissis, P.; Bokobza, L. Glass transition and molecular dynamics in poly (dimethylsiloxane)/silica nanocomposites. *Polymer* **2005**, *46*, 6001−6008.

https://doi.org/10.1021/acsomega.3c00321
ACS Omega 2023, 8, 13911−13919

(39) Belovickis, J.; Macutkevic, J.; Svirskas, Š.; Samulionis, V.; Banys, J.; Shenderova, O.; Borjanovic, V. Ultrasonic and dielectric relaxations in PDMS/ZnO nanocomposite. *Phys. Status Solidi B* **2015**, *252*, 2778−2783.
(40) Sulym, I.; Klonos, P.; Borysenko, M.; Pissis, P.; Gun'ko, V. M. Dielectric and thermal studies of segmental dynamics in silica/PDMS and silica/titania/PDMS nanocomposites. *J. Appl. Polym. Sci.* **2014**.
(41) Cole, K. S.; Cole, R. H. Dispersion and absorption in dielectrics I. Alternating current characteristics. *J. Chem. Phys.* **1941**, *9*, 341−351.
(42) Lionetto, F.; Maffezzoli, A. Polymer characterization by ultrasonic wave propagation. *Adv. Polym. Technol.* **2008**, *27*, 63−73.
(43) Samulionis, V.; Macutkevic, J.; Banys, J.; Belovickis, J.; Shenderova, O. Ultrasonic and dielectric studies of polymer PDMS composites with ZnO and onion-like carbons nanoinclusions. *IOP Conf. Ser.: Mater. Sci. Eng.* **2015**, *87*, 012010.
(44) Streque, J.; Rouxel, D.; Talbi, A.; Thomassey, M.; Vincent, B. Low-Temperature Variation of Acoustic Velocity in PDMS for High-Frequency Applications. *IEEE Trans. Ultrason. Eng.* **2018**, *65*, 862−869.

https://doi.org/10.1021/acsomega.3c00321
ACS Omega 2023, 8, 13911−13919